Biaxial strain-induced transport property changes in atomically tailored SrTiO₃-based systems

Z. Huang,[1] Z. Q. Liu,[1,2] M. Yang,[2] S. W. Zeng,[1,2] A. Annadi,[1,2] W. M. Lü,[1,3] X. L. Tan,[4] P. F. Chen,[4] L. Sun,[1]
X. Renshaw Wang,[1,2] Y. L. Zhao,[1,2] C. J. Li,[1] J. Zhou,[2] K. Han,[1] W. B. Wu,[4] Y. P. Feng,[2] J. M. D. Coey,[1,5]
T. Venkatesan,[1,2,3] and Ariando[1,2,*]

[1]*NUSNNI-NanoCore, National University of Singapore, 117411 Singapore*
[2]*Department of Physics, National University of Singapore, 117542 Singapore*
[3]*Department of Electrical and Computer Engineering, National University of Singapore, 117576 Singapore*
[4]*Hefei National Laboratory for Physical Science at Microscale, University of Science and Technology of China, Hefei 230026,
People's Republic of China*
[5]*School of Physics and CRANN, Trinity College, Dublin 2, Ireland*
(Received 13 April 2014; revised manuscript received 18 August 2014; published 29 September 2014)

Several metallic SrTiO₃-based systems, including reduced SrTiO₃₋δ, Nb-doped SrTiO₃, and two-dimensional electron gas at the LaAlO₃/SrTiO₃(001) interface, have been epitaxially fabricated on various substrates inducing different strain, from −2.98% (compressive) to +0.99% (tensile). For all the SrTiO₃-based systems, strain reduces conductivity. Tensile strain, however, is much more effective at reducing conductivity compared to compressive strain. Further, carrier mobility is found to be more sensitive to strain than carrier density. Calculations based on density functional theory show that strain can break the cubic symmetry of TiO₆ octahedron, lift the degeneracy of Ti $3d$ orbitals, and reduce the number of available states at the bottom of the conduction band to cause low carrier mobility. Our results show the critical features of strain effect on the conducting SrTiO₃-based systems, and shed some light on strain engineering of these functional materials.

I. INTRODUCTION

The family of SrTiO₃-based materials rightfully occupies an important place in modern condensed matter physics. For examples SrTiO₃ has been widely used as a substrate for novel perovskite-oxide devices due to its highly compatible crystal structure and controllable surface termination [1]. Insulating SrTiO₃ films with epitaxial-strain-induced crystal distortion show room-temperature ferroelectricity, paving a new way to trigger ferroelectricity in nonferroelectric materials [2]. Under electrostatic doping by electrical gating, SrTiO₃ can become conducting and exhibit a complex phase diagram [3], with rich physics such as Kondo [4] and Rashba effects [5]. Recently, much attention has been paid to the two-dimensional electron gas (2DEG) at the LaAlO₃/SrTiO₃(001) (LAO/STO) interface [6], where many unexpected functionalities have been observed including two-dimensional superconductivity [7], magnetic order [8], strong spin-orbital coupling [9,10], and coexistence of different electronic phases [11–14]. This diversity of physical properties makes SrTiO₃-based materials of great interest in both scientific research and practical application.

All these interesting properties are believed to be related to the occupancy of Ti $3d$ orbital subbands [15–18], which suggests the possibility of controlling these interesting properties by modulating the Ti orbital occupancy in SrTiO₃-based thin-film devices. Total energy calculations have demonstrated that biaxial epitaxial strain is able to induce TiO₆ octahedral deformation and rotation, which could be effective in controlling orbital degeneracy and band structure in strained SrTiO₃ thin films [19]. Experimental results support the idea that epitaxial strain can not only modulate the functionalities

of ferroelectricity in insulating SrTiO₃ films [2], but also the conducting behavior of the 2DEG at the LAO/STO interface [20]. However, there are still some crucial questions to be answered. Given that all the conducting SrTiO₃-based materials share a similar perovskite structure and Ti t_{2g} conduction band, does biaxial epitaxial strain have the same effect on all those systems? Which factor is more important in strain engineering, the strain amplitude (absolute value of lattice mismatch) or sign (tensile or compressive)? How do carrier density and mobility vary with strain? Here we aim to answer these questions and provide a better understanding of the effect of strain in SrTiO₃.

II. EXPERIMENTAL METHODS

A. Sample preparation

We investigate the effect of biaxial strain on various conducting SrTiO₃-based epitaxial systems, namely, a reduced SrTiO₃₋δ (STO) film prepared under high vacuum, 0.5 wt% Nb-doped SrTiO₃ (NSTO) film with chemically doped carriers, and the 2DEG at the LAO/STO interface epitaxially grown on various substrates. All the films were prepared by the pulsed laser deposition (PLD) method with *in situ* reflection high-energy electron diffraction (RHEED). Before depositing the films, all the substrates used in this work, including LaAlO₃(001) (LAO), (LaAlO₃)₀.₃(Sr₂AlTaO₆)₀.₃₅(001) (LSAT), TiO₂-terminated SrTiO₃(001), and DyScO₃(110) (DSO), were thermally treated to obtain atomically flat surfaces. During growth, the temperature, laser repetition rate, and energy density were fixed at 750 °C, 1–2 Hz, and 1.8 J/cm². The reduced STO and NSTO films were prepared under an oxygen partial pressure of 2×10^{-6} Torr. For their bulk counterparts, reduced STO was prepared by annealing a SrTiO₃ substrate at 750 °C under 2×10^{-6} Torr for 1 h, and

*ariando@nus.edu.sg

a 0.5-wt% doped NSTO substrate was used for bulk NSTO. The conventional LAO/STO interface, where 15 unit cells (uc) of LAO were epitaxially deposited on TiO_2-terminated $SrTiO_3$ substrates, was prepared under 2×10^{-4} Torr. This metallic 2DEG is believed to conduct on the $SrTiO_3$ side of the interface, so it can be considered as the 2DEG in the unstrained $SrTiO_3$ bulk substrate [20]. Epitaxial LAO/STO interfaces, where 15-uc LAO and 15-uc STO layers were grown on different substrates, were prepared under 2×10^{-4} Torr. In this case, the 2DEG lies in the thin strained STO films. Therefore, when compared with the conventional LAO/STO interface, it can present a difference in transport properties due to the difference in the interface strain.

B. Sample characterization

For surface morphology, the samples were examined by atomic force microscopy (AFM, Agilent 5500), and the transport properties were measured by a physical property measurement system (PPMS, Quantum Design) using the van der Pauw method. The crystal structure was characterized by x-ray diffraction (XRD) and reciprocal space mapping (RSM) using Cu Kα_1 radiation ($\lambda = 1.5406$ Å, Panalytical X'pert).

C. Calculation method

All calculations were carried out by using density functional theory (DFT) based Vienna *ab initio* simulation package (VASP) with the Perdew-Burke-Ernzerhof (PBE) approximation for the exchange-correlation functional [21,22]. The frozen-core all-electron projector-augmented wave (PAW) [23] method, as implemented in VASP, was used. The cutoff energy for the expansion of the plane-wave basis was set to 500 eV. The effective on-site Coulomb correction ($U-J = 5.0$ eV and $U-J = 2.0$ eV) was applied to the d-orbital electrons in Ti and Nb atoms, respectively. For $SrTiO_3$ bulk, $8 \times 8 \times 8$ Monkhorst-Pack method generated k-point meshes were used. For Nb-doped $SrTiO_3$, a $2 \times 2 \times 2$ $SrTiO_3$ supercell was used in which one Ti atom was substituted by a Nb atom, and $4 \times 4 \times 4$ k-point meshes were applied. The electronic convergence was set to 1.0×10^{-6} eV, and the force on each atom was optimized smaller than 0.01 eV/Å.

III. RESULTS AND DISCUSSION

The lattice constant of bulk $SrTiO_3$ a_{STO} is 3.905 Å, and the in-plane (pseudo)cubic lattice constant of the other substrates a_{sub} is 3.792 Å for LAO, 3.868 Å for LSAT, and 3.944 Å for DSO, respectively. Hence, as shown in Fig. 1(a), the corresponding lattice mismatch ε [$\varepsilon = (a_{sub} - a_{STO})/a_{sub}$] for $SrTiO_3$-based films is -2.98% on LAO, -0.96% on LSAT, and $+0.99\%$ on DSO, leading to a large *compressive* strain on LAO, a small *compressive* strain on LSAT, and a small *tensile* strain on DSO. Good RHEED oscillations were seen for all the films and for all substrates. The quality of samples can be inferred from Fig. 1. Taking STO/LSAT film, for example, *in situ* RHEED oscillations in Fig. 1(b) demonstrate a good layer-by-layer growth during deposition. Also, the inset AFM image shows clear atomic steps, which indicates a high quality of films. In the XRD θ–2θ scans around (002) shown in Fig. 1(c), all the STO and NSTO films exhibit thickness

fringes from which the calculated film thickness is found to be consistent with that deduced from the RHEED oscillations. More importantly, the epitaxy of heterostructures has been examined by x-ray RSM, where the in-plane and out-of-plane lattice constants can be obtained, as shown in Fig. 1(d), where a typical RSM of around (–103) for a LAO/STO/LSAT heterostructure is presented. The reflections from LAO and STO layers and the LSAT substrate have the same projection along [100]. This directly proves the coherent growth of an LAO/STO interface on LSAT, which means the in-plane lattice constants for the LAO and STO layer and LSAT substrate are the same. This high-quality, coherent growth mode enables us to investigate the biaxial strain effect in the $SrTiO_3$-based systems.

In Fig. 2, we summarize the results of sheet resistance as a function of temperature [$R_S(T)$] for three conducting $SrTiO_3$-based systems with four different strains, ranging from $+0.99\%$ (tensile) to -2.98% (compressive). For their nonstrained counterparts, including the bulk STO, bulk NSTO, and the conventional 2DEG at the interface where LAO layers are grown on $SrTiO_3$ substrates, the metallic behavior is shown in Figs. 2(b), 2(f), and 2(j), respectively. Metallic behavior is suppressed for those strained counterparts, which are characterized by much higher R_S and show insulating behavior at low temperatures. The extent of this suppression depends greatly on the magnitude and sign of the strain. Specifically, on the right side of Fig. 2 representing compressive strain, samples on LSAT substrates, with a smaller lattice mismatch (–0.96%), are always more conducting than those on $LaAlO_3$ with a larger lattice mismatch (from -2.98% to -1.43%, due to a partially relaxed strain in 300-uc STO/LAO). This result seems reasonable if compressive epitaxial strain is responsible for the insulating behavior. However, on the left side of Fig. 2, it can be seen that only a small-amplitude tensile strain from $DyScO_3$ ($+0.99\%$) can make those $SrTiO_3$-based systems even more insulating than those on $LaAlO_3$. In Fig. 3, the AFM image of 300-uc STO/DSO film exhibits clear one-unit-cell-high atomic steps, and no cracks or film discontinuity is observed. Hence the highly insulating state in STO/DSO films should be ascribed to the tensile strain, not other extrinsic factors. And the results shown in Fig. 2 suggest that the strain amplitude is not the only factor that governs the transport properties, and the sign of the strain (compressive or tensile) may be even more important.

The transport properties were investigated in more detail with measurements of sheet carrier density (n_S) and carrier mobility (μ_S). In Fig. 4(a), the carrier densities of 160-uc NSTO films under different strains are almost the same above 100 K, and they are very close to 1.1×10^{15} cm^{-2}, the carrier density induced by 0.5 wt % Nb doping in 160-uc NSTO films. This suggests that strain has little influence on n_S. In contrast, the values of μ_S are very sensitive to strain. As shown in Fig. 4(b), μ_S for NSTO film has its highest value on LSAT with a small compressive strain, a medium value on LAO with a large compressive strain, and is much lower on DSO, where the strain is small but tensile. At 50 K, μ_S of NSTO/DSO is almost 2 orders of magnitude smaller than for NSTO/LSAT. These results suggest that the carrier mobility, which strongly depends on the strain, is the main reason for the insulating state in strained NSTO films. In
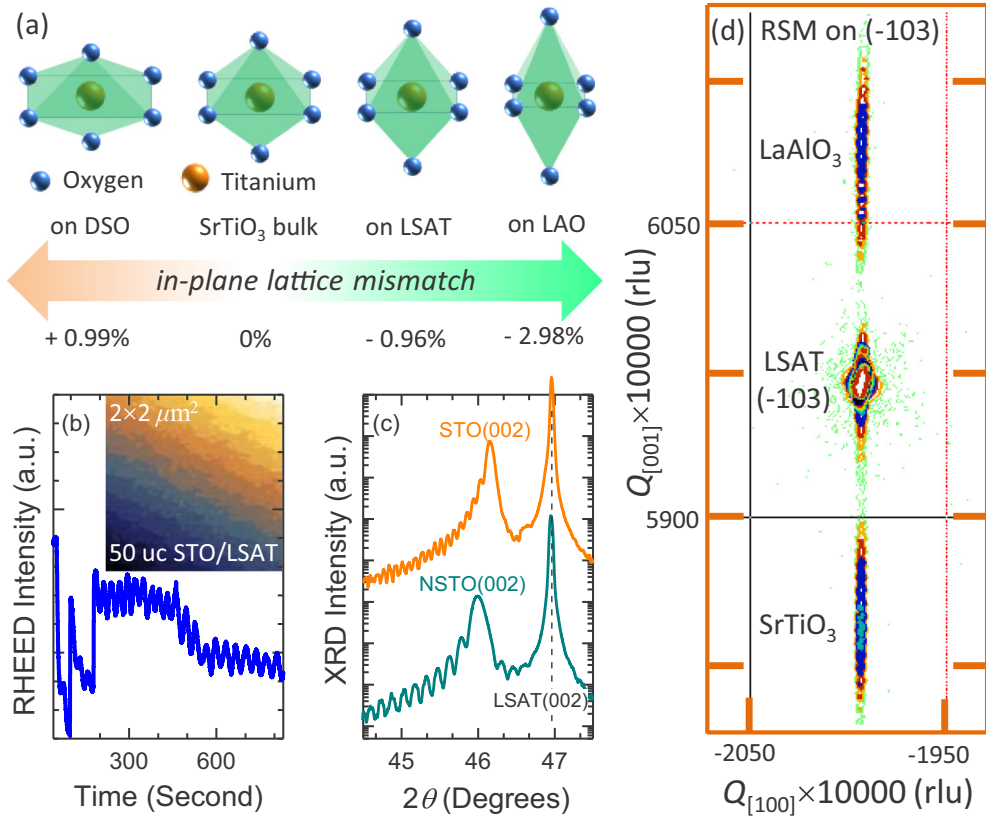
FIG. 1. (Color online) (a) Sketches for tetragonal-like TiO_6 octahedral distortion under different strains. The in-plane expansion and out-of-plane shrinkage are expected under tensile strain, while the opposite distortion can be obtained under compressive strain. (b) *In situ* RHEED oscillation for STO/LSAT heterostructure. (Inset) AFM image for 50-uc STO/LSAT film. (c) XRD $\theta-2\theta$ scans around (002) reflections are shown for 300-uc STO/LSAT and 160-uc NSTO/LSAT samples. (d) RSM around (–103) is shown for LAO (25-uc)/STO(20-uc)/LSAT heterostructure. Note that the units are defined using the absolute lattice constants. For example, for $(hkl) = (-103)$, the projection of LSAT (–103) along the [001] direction $Q_{[003]}$ is 0.597 4, and it can be written as $Q_{[003]} = l\lambda/2a_{[001]}$. Hence the out-of-plane lattice constant for LSAT $a_{[001]} = l\lambda/2Q_{[003]} = (3 \times 1.540\,6\,\text{Å})/(2 \times 0.597\,4) = 3.868\,\text{Å}$.

order to identify whether the carrier mobility is crucial to other SrTiO$_3$-based systems, n_S and μ_S for the 2DEG at the LAO/STO interface are also shown in Figs. 4(c) and 4(d). Due to the highly insulating states for the LAO/STO interface under tensile strain [20], we can only compare the conventional LAO/STO interfaces with ones under compressive strain. As is clearly shown in Fig. 4(c), the 2DEG in the strained SrTiO$_3$ layer can even have higher n_S than the conventional one, depending on the SrTiO$_3$ layer thickness, which influences the position of the mobility edge with respect to the Fermi level in epitaxial LAO/STO interfaces [24]. Especially at 2 K, when the thermally activated carriers from oxygen vacancies are "frozen out" [25,26], the n_S of 2DEG at the bottom of the conduction band in the LAO/STO/LSAT sample can be 1 order of magnitude larger than in the conventional interface. However, μ_S of compressively strained 2DEG is found to be reduced by 3–4 orders of magnitude in Fig. 4(d) at low temperatures, resulting in the much higher resistance in the epitaxial LAO/STO interface.

Based on these results, two common features of electronic transport for strained SrTiO$_3$-based systems can be summarized. *First*, the metallic state that is dominant in the bulk is greatly suppressed by strain, especially by tensile strain. *Second*, the carrier mobility μ_S is very sensitive to strain,

and this is the main reason for the observed changes in strain-mediated conductivity.

In order to further demonstrate the relationship among transport properties, strain states, and crystal structures, we studied STO/LSAT films with different thicknesses. As revealed by $R_S(T)$ in Fig. 5(a), when the films are thin, the values of R_S are very large and insulating behavior ($dR_S/dT < 0$) is observed over the whole temperature range (2–300 K). By increasing the film thickness to 300 uc, the bulklike metallic behavior is recovered above 180 K with $dR_S/dT > 0$. But the insulating phase still dominates at low temperatures, probably due to the "carrier freeze-out" effect that is reported even in the micrometer-thick STO films [25]. Figure 5(b) shows the room-temperature sheet conductance as a function of STO thickness. When the thickness is less than 30 uc, samples are highly insulating and the sheet resistance is out of our measurement range; similar phenomena have also been reported elsewhere [27,28]. If the sheet conductance G_S can be estimated by $G_S = k(t - t_D)$, where k is a constant, t is the film thickness, and t_D is the thickness for the completely insulating STO layer, t_D of STO/LSAT (~ 45 uc) can be obtained by fitting the data in Fig. 5(b). The conductivity increases with film thickness at 200 K, as shown in the inset of Fig. 5(b), again supporting the gradual recovery of bulk SrTiO$_{3-\delta}$ conductance in the
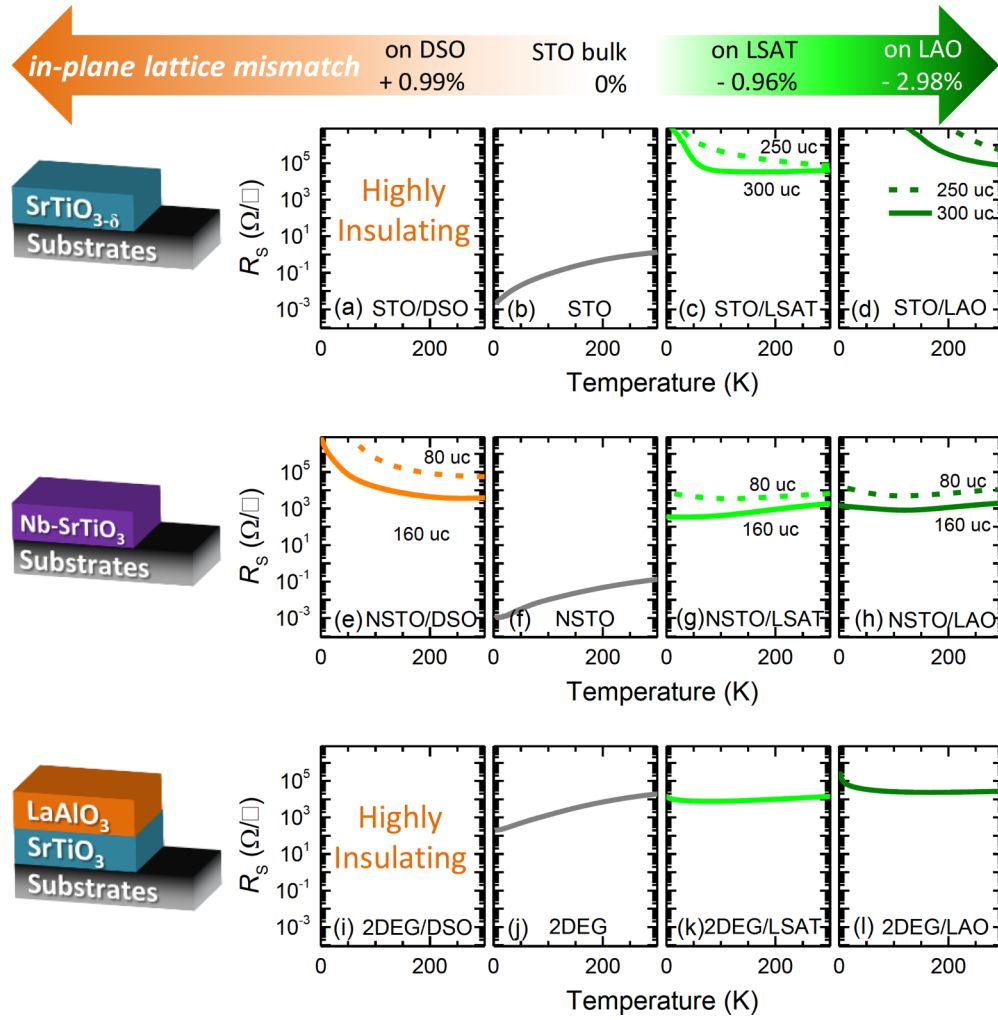
FIG. 2. (Color online) $R_S(T)$ curves for STO in (a)–(d), NSTO in (e)–(h), and 2DEG at the LAO/STO interface (i)–(l), under different strain states from tensile (left) to compressive (right).

thicker films. This thickness-dependent phenomenon can be also observed in STO and NSTO films on other substrates, as shown in Fig. 2. Normally, increasing film thickness is an

effective way to relax strain. This is true for SrTiO$_3$-based samples grown on LAO substrate. As expected, the in-plane compressive strain is reduced from -2.98% to -1.43% when
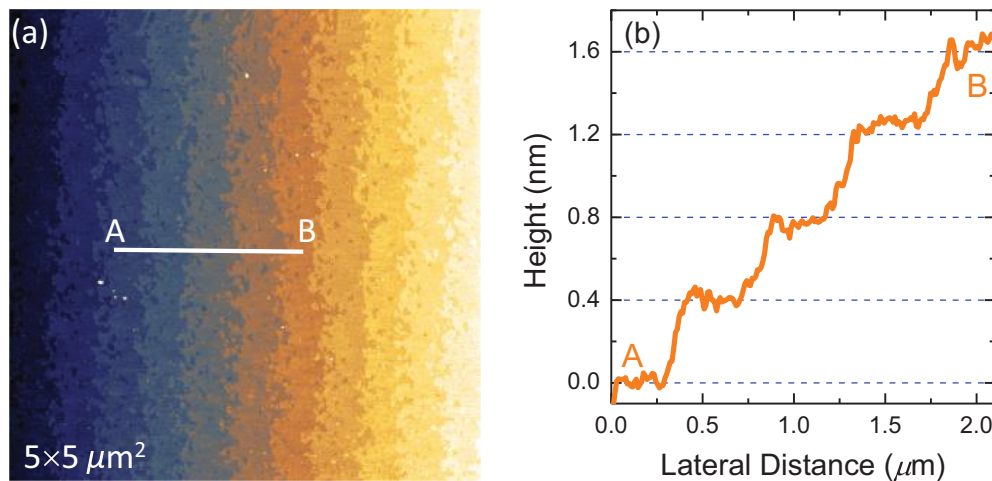

FIG. 3. (Color online) (a) AFM image of 300-uc SrTiO$_3$/DyScO$_3$ films. (b) Height profile along line AB shown in (a). Clearly, the film exhibits a smooth surface where the step height is around 1 uc (~ 0.4 nm), and no crack or film discontinuity was found in our AFM measurement.
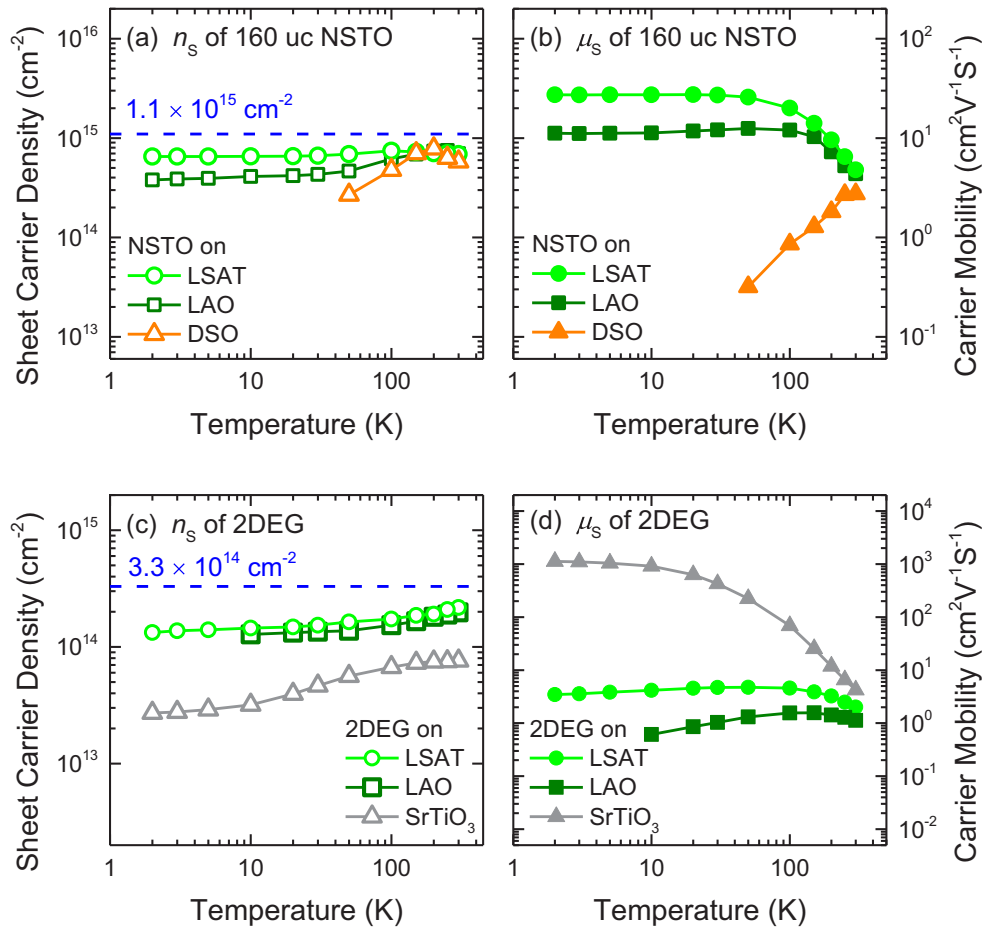
FIG. 4. (Color online) Sheet carrier density n_S and mobility μ_S for 160-uc NSTO on different substrates are shown in (a) and (b), respectively. The blue-dashed line in (a) denotes the value of carrier density calculated based on 0.5 wt% Nb doping in 160-uc NSTO film. And for the 2DEG at an epitaxially grown LAO(15-uc)/STO(12-uc) interface, the sheet carrier density and mobility are also shown in (c) and (d), respectively. The conventional 2DEG with 15-uc LAO film on STO substrate is also plotted for comparison. The blue-dashed line in (c) denotes the value of carrier density required to prevent polar catastrophe at the LAO/STO interface.

film thickness is increased from 60 to 300 uc, according to the RSM around (103) (not shown). However, the XRD data indicate there is no such in-plane strain relaxation in our STO/LSAT films up to 300 uc. As shown in $\theta - 2\theta$ scans of Fig. 5(c), when increasing the STO film thickness from 60 to 300 uc, the 2θ of STO(002) peaks shifts from 46.031(5) to 46.153(5) °, corresponding to the decrease of the out-of-plane lattice constant $a_{[001]}$ from 3.940(1) to 3.930(1) Å. On the other hand, the RSM around (−103) reflection in Fig. 5(d) illustrates the preservation of coherent growth with $a_{[100]} = a_{LSAT}$, and there is *no* observable in-plane lattice relaxation even in 300-uc-thick STO/LSAT film.

For cubic perovskite $SrTiO_3$, the biaxial compressive strain can cause two types of structural distortion. One is the tetragonal-like distortion on each TiO_6 octahedron, which can increase (decrease) the out-of-plane (in-plane) lattice constant and thus lift the Ti $3d$ orbital degeneracy. The other one is the octahedral rotation in TiO_6 network, which will change the Ti-O-Ti bond angle but not Ti-O band length. For the perovskite oxides, the in-plane octahedral structure can be described by

$$d_{\text{Ti-O}} = (1/2)a_{[100]}/\sin(\beta/2) \qquad (1)$$

and

$$\alpha = 90° - \beta/2, \qquad (2)$$

where $d_{\text{Ti-O}}$ is the in-plane Ti-O band length, $a_{[100]}$ is the in-plane lattice constant, β is the in-plane Ti-O-Ti bond angle, and α is the in-plane rotation angle for TiO_6 octahedron. On the other hand, the out-of-plane lattice constant $a_{[100]}$ can be evaluated by the Poisson effect induced by biaxial compressive strain with

$$\Delta a_{[001]} = a_{[001]} - a_{\text{STO}} = -4\upsilon \Delta d_{\text{Ti-O}}/(1-\upsilon)$$
$$= [(a_{[100]}/\cos\alpha) - \alpha_{\text{STO}}][2\upsilon/(\upsilon - 1)], \qquad (3)$$

where υ is the Poisson ratio of a single TiO_6 octahedron. If assuming α in the 60-uc STO layer is 0, the relative rotation angle α' can be calculated accordingly. The evolution of the $a_{[001]}/a_{[100]}$ ratio (representing the tetragonal-like distortion) and the rotation angle α' are shown in Fig. 5(e). When the STO/LSAT film is very thin, the compressive strain from the LSAT substrate mainly contributes to the tetragonal-like distortion in STO film. For the thick films where coherent growth is still preserved, the octahedral rotation is enhanced while the tetragonal distortion is weakened, accompanied
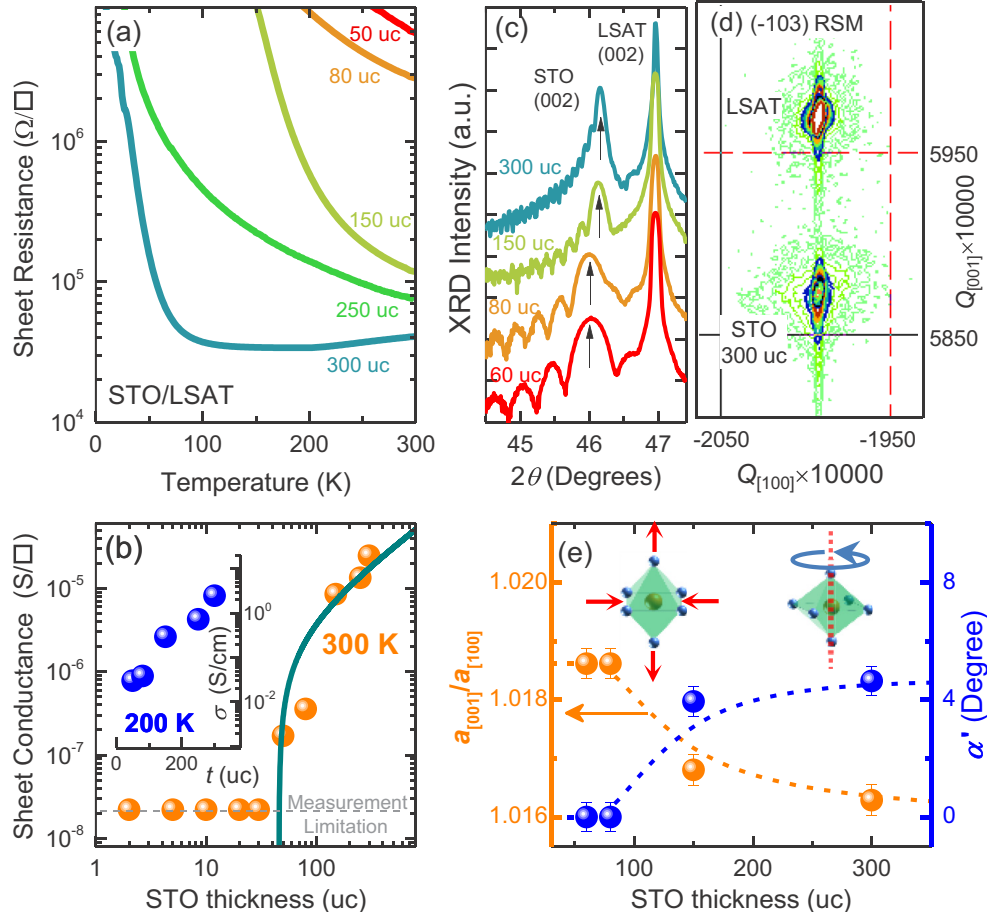
FIG. 5. (Color online) (a) $R_S(T)$ curves for STO/LSAT films with different film thicknesses. (b) Room-temperature sheet conductance for STO/LSAT films at different thicknesses, and the dark cyan line is fitted by assuming t_D is 45 uc. (Inset) Conductivity as a function of STO/LSAT thickness at 200 K. (c) XRD $\theta-2\theta$ scans around (002) reflections for STO/LSAT films from 60 to 300 uc. (d) RSM around (−103) for 300-uc STO/LSAT films, where the film and substrate share the same projection along [100] orientation, indicating coherent growth. (e) The $a_{[001]}/a_{[100]}$ ratio (indicating the octahedral tetragonal distortion) and angle α' (denoting the octahedral rotation) are shown as a function of STO/LSAT film thickness.

by the gradual recovery of conducting behavior. Next, the origins of the insulating behavior and low mobility in those strained SrTiO$_3$-based materials, especially under the tensile strain, are discussed in terms of the strain-induced distortion of the TiO$_6$ octahedra and its subsequent impact. First, let us consider the effect of octahedral rotation on transport properties. Generally, the octahedral rotation is expected to occur under compressive not tensile strain. The conduction bandwidth W, which depends on the overlap integrals between the Ti 3d and O 2p orbitals, is closely related to such rotation, i.e., $W \propto \cos \alpha/d_{\text{Ti-O}}^{3.5} \propto \cos^{4.5} \alpha$ [29,30]. When changing the STO/LSAT film thickness from 60 to 300 uc, α' is increased by almost 5°, corresponding to only a 2% reduction on W. However, the conductivity is increased almost by 2 orders of magnitude, suggesting that the insulating behavior of STO/LSAT should not be ascribed to the octahedral rotation. Therefore the effect of tetragonal-like distortion and its subsequent impact on orbitals in strained STO layers should be emphasized [31]. As shown in Fig. 6(a), when the epitaxial biaxial strain is applied to the TiO$_6$ octahedron, the

cubic crystal symmetry is broken by tensile (compressive) strain with in-plane lattice expansion (shrinkage). Thus the degeneracy of t_{2g} orbitals is lifted and the energy of 3d_{xy} (3$d_{yz/zx}$) orbitals becomes lowest under tensile (compressive) strain due to the coupling between orbitals and the crystal field. DFT calculations in Fig. 5(b) also confirm this raising of the t_{2g} orbital degeneracy around the bottom of the conduction band (E_{CB}) caused by strain. In other words, the number of degenerate orbitals around E_{CB} is reduced from three in SrTiO$_3$ bulk to one (two) by tensile (compressive) strain. This loss of orbital degeneracy will narrow the total density of state (DOS) at the bottom of the conduction band, resulting in low-mobility states [32]. As shown in Figs. 6(c) and 6(d), for both the SrTiO$_3$ and Nb − SrTiO$_3$ cases, the DOS around the bottom of the conduction band (E_{CB}) is narrowest under tensile strain and broadest without strain. This is consistent with our experimental observations that the carrier mobility is lowest under tensile strain and highest without strain. It also explains why electron localization is more effective under tensile as opposed to compressive strain.
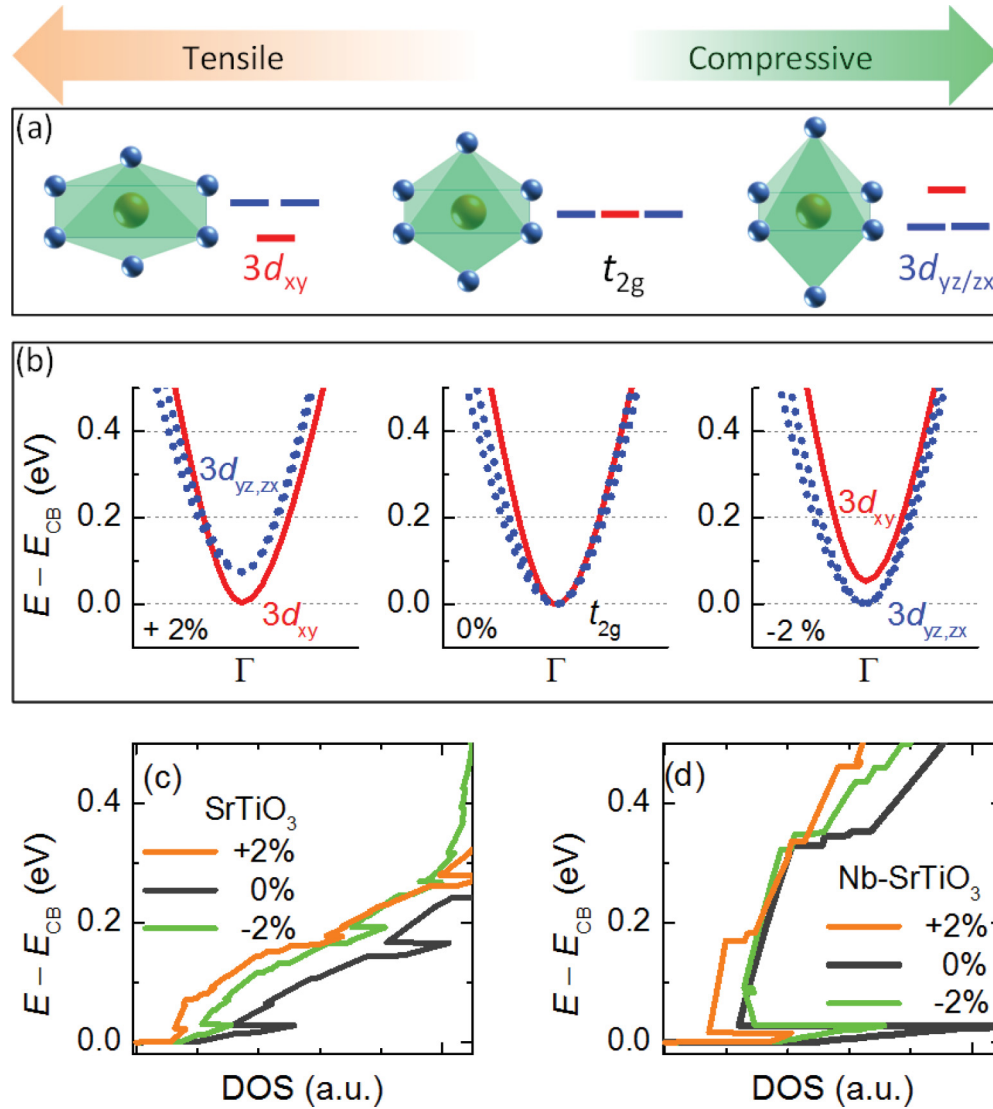
FIG. 6. (Color online) (a) Lifting Ti t_{2g} orbital degeneracy by strain-induced TiO_6 distortion. (b) The DFT-calculated band structure of $SrTiO_3$ under different strain states (+2% tensile strain, 0% no strain, and −2% compressive strain). DFT-calculated DOS of the conduction band for $SrTiO_3$ in (c) and $SrTi_{7/8}Nb_{1/8}O_3$ in (d). The energy is denoted with respect to the bottom of the conduction band E_{CB}.

IV. CONCLUSIONS

In summary, biaxial strain effects in three different conducting $SrTiO_3$-based systems, including the reduced STO, NSTO, and conducting LAO/STO interface, have been systemically investigated. Two common features emerge. One is the reduction of conductivity in strained samples, especially for samples under tensile strain. The other is that the carrier mobility is more sensitive to the strain than carrier density, leading to a reduction in conductivity. The degeneracy of the orbitals of octahedrally coordinated Ti is more effectively modified under tensile rather than compressive strain, resulting in lower mobility and hence lower conductivity. Our results clearly demonstrate that biaxial strain, especially the sign of the strain, plays an important role in controlling conductivity in $SrTiO_3$-based systems, which will be of importance for future oxide electronic devices.

[1] M. Kawasaki, K. Takahashi, T. Maeda, R. Tsuchiya, M. Shinohara, O. Ishiyama, T. Yonezawa, M. Yoshimoto, and H. Koinuma, Science **266**, 1540 (1994).

[2] J. H. Haeni, P. Irvin, W. Chang, R. Uecker, P. Reiche, Y. L. Li, S. Choudhury, W. Tian, M. E. Hawley, and B. Craigo, Nature (London) **430**, 758 (2004).

[3] Y. Lee, C. Clement, J. Hellerstedt, J. Kinney, L. Kinnischtzke, X. Leng, S. D. Snyder, and A. M. Goldman, Phys. Rev. Lett. **106**, 136809 (2011).

[4] M. Lee, J. R. Williams, S. Zhang, C. D. Frisbie, and D. Goldhaber-Gordon, Phys. Rev. Lett. **107**, 256601 (2011).

[5] H. Nakamura, T. Koga, and T. Kimura, Phys. Rev. Lett. **108**, 206601 (2012).

[6] A. Ohtomo and H. Y. Hwang, Nature (London) **427**, 423 (2004).

[7] N. Reyren, S. Thiel, A. D. Caviglia, L. F. Kourkoutis, G. Hammerl, C. Richter, C. W. Schneider, T. Kopp, A.-S. Rüetschi, D. Jaccard, M. Gabay, D. A. Muller, J.-M. Triscone, and J. Mannhart, Science **317**, 1196 (2007).

[8] A. Brinkman, M. Huijben, M. van Zalk, J. Huijben, U. Zeitler, J. C. Maan, W. G. van der Wiel, G. Rijnders, D. H. A. Blank, and H. Hilgenkamp, Nature Mater. **6**, 493 (2007).

[9] A. D. Caviglia, M. Gabay, S. Gariglio, N. Reyren, C. Cancellieri, and J.-M. Triscone, Phys. Rev. Lett. **104**, 126803 (2010).

[10] M. Ben Shalom, M. Sachs, D. Rakhmilevitch, A. Palevski, and Y. Dagan, Phys. Rev. Lett. **104**, 126802 (2010).

[11] Ariando, X. Wang, G. Baskaran, Z. Q. Liu, J. Huijben, J. B. Yi, A. Annadi, A. Roy Barman, A. Rusydi, S. Dhar, Y. P. Feng, J. Ding, H. Hilgenkamp, and T. Venkatesan, Nature Commun. **2**, 188 (2011).

[12] D. A. Dikin, M. Mehta, C. W. Bark, C. M. Folkman, C. B. Eom, and V. Chandrasekhar, Phys. Rev. Lett. **107**, 056802 (2011).

[13] L. Li, C. Richter, J. Mannhart, and R. C. Ashoori, Nature Phys. **7**, 762 (2011).

[14] J. A. Bert, B. Kalisky, C. Bell, M. Kim, Y. Hikita, H. Y. Hwang, and K. A. Moler, Nature Phys. **7**, 767 (2011).

[15] M. Salluzzo, J. C. Cezar, N. B. Brookes, V. Bisogni, G. M. De Luca, C. Richter, S. Thiel, J. Mannhart, M. Huijben, A. Brinkman, G. Rijnders, and G. Ghiringhelli, Phys. Rev. Lett. **102**, 166804 (2009).

[16] Z. S. Popović, S. Satpathy, and R. M. Martin, Phys. Rev. Lett. **101**, 256801 (2008).

[17] P. Delugas, A. Filippetti, V. Fiorentini, D. I. Bilc, D. Fontaine, and P. Ghosez, Phys. Rev. Lett. **106**, 166807 (2011).

[18] A. F. Santander-Syro, O. Copie, T. Kondo, F. Fortuna, S. Pailhès, R. Weht, X. G. Qiu, F. Bertran, A. Nicolaou, A. Taleb-lbrahimi, P. Le Fèvre, G. Herranz, M. Bibes, N. Reyren, Y. Apertet, P. Lecoeur, A. Barthélémy, and M. J. Rozenberg, Nature (London) **469**, 189 (2011).

[19] R. F. Berger, C. J. Fennie, and J. B. Neaton, Phys. Rev. Lett. **107**, 146804 (2011).

[20] C. W. Bark, D. A. Felker, Y. Wang, Y. Zhang, H. W. Jang, C. M. Folkman, J. W. Park, S. H. Baek, H. Zhou, D. D. Fong, X. Q. Pan, E. Y. Tsymbal, M. S. Rzchowski, and C. B. Eom, Proc. Natl. Acad. Sci. USA **108**, 4720 (2011).

[21] G. Kresse and J. Hafner, Phys. Rev. B **47**, 558(R) (1993).

[22] G. Kresse and J. Hafner, Phys. Rev. B **48**, 13115 (1993).

[23] P. E. Blöchl, Phys. Rev. B **50**, 17953 (1994).

[24] Z. Huang, X. R. Wang, Z. Q. Liu, W. M. Lü, S. W. Zeng, A. Annadi, W. L. Tan, X. P. Qiu, Y. L. Zhao, M. Salluzzo, J. M. D. Coey, T. Venkatesan, and Ariando, Phys. Rev. B **88**, 161107(R) (2013).

[25] Z. Q. Liu, D. P. Leusink, X. Wang, W. M. Lü, K. Gopinadhan, A. Annadi, Y. L. Zhao, X. H. Huang, S. W. Zeng, Z. Huang, A. Srivastava, S. Dhar, T. Venkatesan, and Ariando, Phys. Rev. Lett. **107**, 146802 (2011).

[26] Z. Q. Liu, C. J. Li, W. M. Lü, X. H. Huang, Z. Huang, S. W. Zeng, X. P. Qiu, L. S. Huang, A. Annadi, J. S. Chen, J. M. D. Coey, T. Venkatesan, and Ariando, Phys. Rev. X **3**, 021010 (2013).

[27] T. Hernandez, C. W. Bark, D. A. Felker, C. B. Eom, and M. S. Rzchowski, Phys. Rev. B **85**, 161407 (2012).

[28] P. Brinks, W. Siemons, J. E. Kleibeuker, G. Koster, G. Rijnders, and M. Huijben, Appl. Phys. Lett. **98**, 242904 (2011).

[29] M. Medarde, J. Mesot, P. Lacorre, S. Rosenkranz, P. Fischer, and K. Gobrecht, Phys. Rev. B **52**, 9248 (1995).

[30] P. G. Radaelli, G. Iannone, M. Marezio, H. Y. Hwang, S-W. Cheong, J. D. Jorgensen, and D. N. Argyriou, Phys. Rev. B **56**, 8265 (1997).

[31] W. Wunderlich, H. Ohta, and K. Koumoto, Physica B **404**, 2202 (2009).

[32] N. F. Mott and E. A. Davis, *Electronic Processes in Non-Crystalline Materials* (Clarendon Press, Oxford, 1971).